Internalization of Red Blood Cell-Mimicking Hydrogel Capsules with pH-Triggered Shape Responses

Veronika Kozlovskaya,[†,⊥] Jenolyn F. Alexander,[§,⊥] Yun Wang,[†] Thomas Kuncewicz,[§] Xuewu Liu,[§] Biana Godin,[§,∥,*] and Eugenia Kharlampieva[†,‡,∥,*]

[†]Department of Chemistry, University of Alabama at Birmingham, Birmingham, Alabama 35294, United States, [‡]Center for Nanoscale Materials and Biointegration, University of Alabama at Birmingham, Birmingham, Alabama 35294, United States, and [§]Department of Nanomedicine, Houston Methodist Research Institute, Houston, Texas 77030, United States. [⊥]V. Kozlovskaya and J. F. Alexander equally contributed. [∥]B. Godin and E. Kharlampieva share equal seniority.

ABSTRACT We report on naturally inspired hydrogel capsules with pH-induced transitions from discoids to oblate ellipsoids and their interactions with cells. We integrate characteristics of erythrocytes such as discoidal shape, hollow structure, and elasticity with reversible pH-responsiveness of poly(methacrylic acid) (PMAA) to design a new type of drug delivery carrier to be potentially triggered by chemical stimuli in the tumor lesion. The capsules are fabricated from cross-linked PMAA multilayers using sacrificial discoid silicon templates. The degree of capsule shape transition is controlled by the pH-tuned volume change, which in turn is regulated by the capsule wall composition. The $(PMAA)_{15}$ capsules undergo a dramatic 24-fold volume change, while a moderate 2.3-fold volume variation is observed for more rigid PMAA—(poly(*N*-vinylpyrrolidone) $(PMAA—PVPON)_5$ capsules when solution pH is varied between 7.4 and 4. Despite that both types of capsules exhibit discoid-to-oblate ellipsoid transitions, a 3-fold greater swelling in radial dimensions is found for one-component systems due to a greater degree of the circular face bulging. We also show that $(PMAA—PVPON)_5$ discoidal capsules interact differently with J774A.1 macrophages, HMVEC endothelial cells, and 4T1 breast cancer cells. The discoidal capsules show 60% lower internalization as compared to spherical capsules. Finally, hydrogel capsules demonstrate a 2-fold decrease in size upon internalization. These capsules represent a unique example of elastic hydrogel discoids capable of pH-induced drastic and reversible variations in aspect ratios. Considering the RBC-mimicking shape, their dimensions, and their capability to undergo pH-triggered intracellular responses, the hydrogel capsules demonstrate considerable potential as novel carriers in shape-regulated transport and cellular uptake.

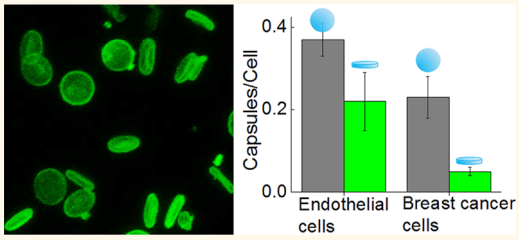

KEYWORDS: discoidal capsules · layer-by-layer · multilayer hydrogels · pH-responsive shapes · cellular uptake

The majority of blood-borne objects in Nature have nonspherical shape and enhanced elasticity, which affect their biophysical characteristics and particularly their transport across the biobarriers. The ability of erythrocytes to reversibly deform in the hydrodynamic flow allows efficient navigation within blood vessels of varying diameter and flow rates, while a decrease in the erythrocyte membrane deformability serves as a trigger for their clearance from the circulation.[1−3] Metastatic cancer cells have a higher degree of elasticity than healthy cells, a characteristic that is believed to be integral to their ability to efficiently transport to new locations.[4]

Replicating the nature, geometry, and elasticity of synthetic carriers has been optimized to regulate their interactions with biological substances.[5−8] *In vitro* studies showed the importance of carrier geometry in endocytosis, vesiculation, phagocytic internalization, and adhesion to the target receptors.[9−15] *In vivo*, nonspherical nano- and microparticles with a higher aspect ratio, such as rods and discs, demonstrated increased blood circulation and enhanced adhesion to endothelium under flow.[16−19] Discoidal particles have been shown to exhibit a significantly better margination ability compared to spherical particles, which allows for sensing biological deviances more efficiently.[20] Godin *et al.* have previously reported a 5-fold higher accumulation of silicon discs in breast tumor xenografts as compared to their spherical counterparts of the same dimensions.[21] A few works have pointed out the importance

* Address correspondence to ekharlam@uab.edu; bgodin@houstonmethodist.org.

Received for review January 25, 2014 and accepted May 21, 2014.

Published online May 21, 2014
10.1021/nn500512x

of the particle elasticity for minimizing phagocytosis by macrophages and increasing particle lifetime in the body. Red blood cell (RBC)-mimicking hydrogel microparticles have demonstrated an increased circulation time due to their high deformability.[16] Macrophages were less able to take up softer particles than the rigid ones,[22] while hepatic carcinoma cells (HepG2) exhibited a more efficient internalization kinetics and magnitude in the case of softer hydrogel particles as compared to the stiffer, highly cross-linked particles of the same composition.[23] Despite the variety of particle geometries and elasticities, the dynamic control over carrier properties remains a big challenge due to synthetic and instrumental difficulties that hinder integration of stimuli-responsiveness into shaped structures. However, as in Nature, the ability of carriers to adapt their physicochemical properties would be crucial for successful drug delivery.

The layer-by-layer (LbL) technique allows not only synthetically recreating the shape and elasticity of cellular elements found in the circulation but also imparting responsiveness to physicochemical impulses.[24−29] The LbL technique involves a sequential assembly of polymers onto sacrificial substrates followed by substrate dissolution.[30−35] The resulting hollow particles (capsules) comprise ultrathin multilayer shells (<50 nm) and sub-micrometer- or micrometer-size cavities used for loading and controlled delivery of functional cargo.[36−39] This technique offers unique advantages of fabrication on various substrates with nanoscale control over thickness, composition, structure, and properties.[40−44] Nonspherical capsules with complex shapes have been obtained as replicas of biological structures or anisotropic inorganic microparticles.[32,45−51] To prevent capsules from environmentally triggered dissolution, electrostatically bonded or hydrogen-bonded multilayer shells can be chemically cross-linked.[52−55] RBC-mimicking discoidal capsules, recently fabricated by Gao and co-workers by stepwise cross-linking of poly(allylamine hydrochloride), showed oxygen-carrying properties and recovery after deformation in narrow microcapillaries.[56] If composed of stimuli-sensitive polymers, cross-linked capsules can exhibit reversible hydrogel-like swelling/shrinkage behavior due to disruption of interchain associations not involved in covalent cross-links.[54,57] As controlled by the pH-responsive wall, hydrogel capsules, *e.g.*, made of cross-linked poly(methacrylic acid) (PMAA), can undergo sharp volume transitions by 2-fold swelling in response to a pH increase, leading to swollen, thermodynamically stable structures.[54] This increase in volume is due to the uncompensated electrostatic repulsion between COO^- groups at basic pH, as well as the osmotic pressure caused by an influx of counterions acting to compensate excess charge. Thus, these capsules represent a unique example of fluid encapsulated by a stimuli-responsive nanothin hydrogel wall. Importantly, PMAA hydrogel capsules have been recently found to be nontoxic with a potential for many biomedical applications such as anticancer drug and vaccine delivery vehicles both *in vitro* and *in vivo*.[58,59]

Although pH-responsive hydrogel multilayer-derived capsules have been investigated for a decade, these studies were mostly limited to spherical systems.[54,55] The existing literature on nonspherical hydrogel capsules focuses on the static state of the capsules, while disregarding capsule stimuli-sensitivity.[49] The lack of knowledge on responsive behavior of nonspherical capsules can be explained by the technical difficulties in synthesizing shaped capsules with stimuli-sensitive walls. We have lately synthesized cubical hydrogel capsules of cross-linked PMAA with pH-switchable geometries controlled by chemical composition of capsule walls.[60,61] In those studies, PMAA capsules changed their shape from cubical to spherical when transitioned from pH = 3 to pH = 8, while PMAA/poly(*N*-vinylpyrrolidone) (PMAA/PVPON) capsules retained their cubical shape and increased in size instead under those conditions. PVPON is biocompatible and has been used in drug delivery.[62,63] As known, the biocompatibility of materials can be improved by increasing their hydrophilicity, *e.g.*, through introducing hydrophilic macromolecules such as poly(ethylene glycol) (PEG). The hydrophilicity mainly helps inhibit protein adsorption and cell recognition. Similarly to PEG, PVPON has been recently shown to prevent protein absorption on the surfaces due to its very hydrophilic nature and affect phagocytosis and the pharmacokinetics of PVPON-coated polymeric particles *in vitro* and *in vivo*.[64,65] Gaucher *et al.* have also demonstrated that the percentage of PVPON-coated particles trapped in the RES organs was smaller than that for the PEGylated particles.[65]

In the current work we report on Nature-inspired pH-responsive hydrogel capsules of discoidal shape and their interactions with cells of various origins. We are motivated by the fact that the elasticity and shape of polymer particles are expected to affect the transport characteristics across biological barriers.[9,66] In our study we integrate characteristics of erythrocytes such as discoidal shape, hollow structure, and elasticity with the reversible pH-responsiveness of PMAA to design a new type of drug delivery carrier to be potentially triggered by chemical stimuli in the tumor lesion. In fact, the extracellular pH of malignant tumors is acidic (pH = 6.5−5.0) compared to normal tissue (pH = 7.2−7.4).[9,10] We investigate pH-triggered size changes of discoidal and spherical capsules corresponding to varying capsule wall rigidity, alongside its impact on capsule interactions with cells. Internalization of these capsules by J774A.1 macrophages, HMVEC endothelial cells, and 4T1 breast cancer cells is compared to that for the correspondingly shaped solid cores. Our study opens new avenues in the field of shape- and

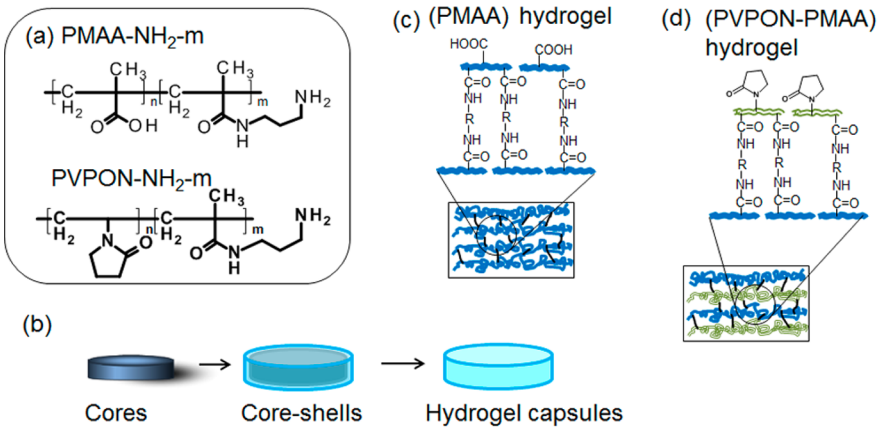

Scheme 1. (a) Chemical structures of poly(methacrylic acid-*co*-(aminopropyl)methacrylamide) (PMAA-NH_2-5) and poly-(*N*-vinylpyrrolidone-*co*-(aminopropyl)methacrylamide) (PVPON-NH_2-7) copolymers used for capsule fabrication. (b) Schematics for fabrication of two types of hydrogel capsules including PMAA and PMAA−PVPON obtained from hydrogen-bonded PMAA-NH_2/PVPON and PVPON-NH_2/PMAA multilayers, respectively, through carbodiimide-assisted cross-linking. In PMAA capsules (c), PVPON is released from the hydrogel film upon cross-linking, while in PMAA−PVPON (d), PVPON-NH_2 chains are cross-linked to PMAA. 'R' denotes three methylene groups.

elasticity-induced cellular uptake of therapeutic triggers to be potentially developed into a novel and powerful delivery method with broad applications in cancer therapy.

RESULTS AND DISCUSSION

The pH-sensitive hydrogel capsules of cross-linked PMAA were fabricated as hollow replicas of discoid silicon templates (Scheme 1). Monodisperse silicon discs with a large aspect ratio, defined as the ratio of the largest to smallest dimensions (length, $L = 2.68 \pm 0.07$ μm; height, $H = 0.45 \pm 0.08$ μm) were used as sacrificial templates (Figure 1). Two types of discoidal capsules denoted as single-component (PMAA) and two-component (PMAA−PVPON) were prepared (Scheme 1). To produce these capsules, copolymers of PMAA or PVPON bearing a known amount of amino-containing cross-linked centers were synthesized and used for hydrogen-bonded multilayer assembly on silicon discs at pH = 2.6 followed by 1-ethyl-3-(3-(dimethylamino)propyl)carbodiimide hydrochloride (EDC)-assisted cross-linking and core dissolution (see Experimental Methods for details). The chemical structures of poly(methacrylic acid-*co*-(aminopropyl)-methacrylamide) (PMAA-NH_2-5) and poly(*N*-vinylpyrrolidone-*co*-(aminopropyl)methacrylamide) (PVPON-NH_2-7) copolymers with a certain molar percentage of amino-group-containing polymer units are shown in Scheme 1a.

In the case of PMAA capsules, PMAA-NH_2-5 copolymer was assembled with PVPON homopolymer *via* hydrogen bonding interactions into (PMAA-NH_2-5/PVPON)$_{15}$ shells, where the subscript denotes the number of polymer bilayers in the multilayer. One-component (PMAA)$_{15}$ capsules were obtained by exposure of (PMAA-NH_2-5/PVPON)$_{15}$ core−shells to EDC, resulting in amide linkages between amino and carboxylic groups of PMAA-NH_2-5 layers and PVPON removal (Scheme 1c).

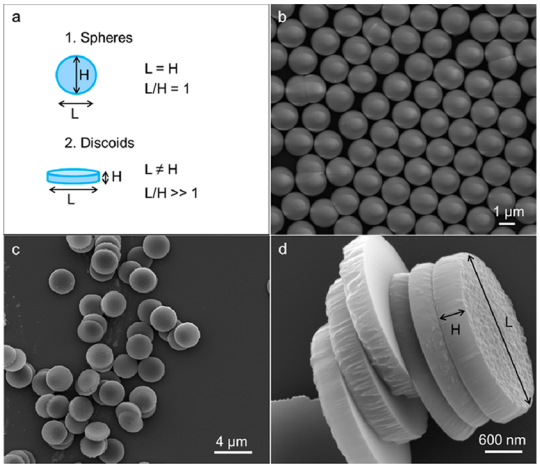

Figure 1. Schematics of spherical and discoid sacrificial templates used for fabrication of multilayer hydrogel capsules (a). SEM images of spherical 1.8 μm silica particles (b) and silicon discoids (c, d) used as sacrificial templates.

To fabricate two-component PMAA−PVPON hydrogel capsules, PMAA homopolymer was assembled with PVPON-NH_2-7 into (PMAA/PVPON-NH_2-7)$_5$ followed by EDC-assisted cross-linking (Scheme 1d). In both cases, the number of cross-links is controlled by the number of monomer units with amino groups in the copolymer.[61]

Dissolution of the cores in acidic media resulted in formation of hydrogel capsules with well-defined discoidal shapes at pH = 4 (Figure 2). Remarkably, both types of capsules are capable of preserving the high-aspect-ratio geometry of discs despite the ultrathin capsule walls. The (PMAA)$_{15}$ and (PMAA−PVPON)$_5$ hydrogel walls have an average bilayer thickness of 7.4 ± 0.2 nm and 7.2 ± 0.5 nm per bilayer, respectively, as measured by ellipsometry using flat films deposited on silicon wafers (see Experimental Methods for details). Changing the solution pH from 4 to 7.4 results in increased sizes of both types of capsules (Figure 2).

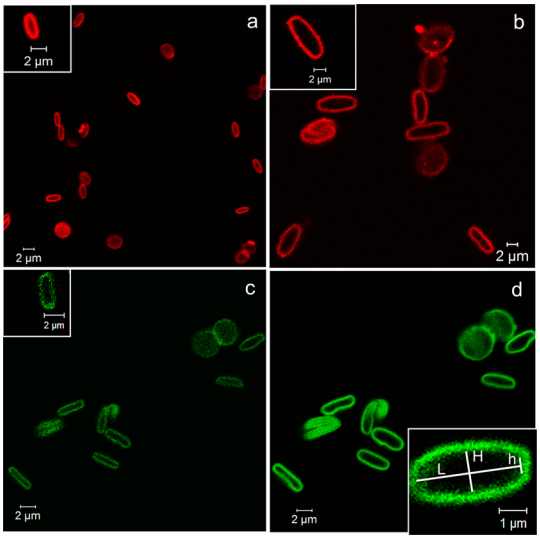

Figure 2. Confocal microscopy images of discoidal $(PMAA)_{15}$ (a, b) and $(PMAA-PVPON)_5$ (c, d) hydrogel capsules at pH = 4 (a, c) and pH = 7.4 (b, d). Insets show a cross-section of individual multilayer hydrogel capsules. Inset in (d) demonstrates the dimensional analysis of the analyzed discoidal capsules including capsule diameter, *L*, maximum cross-sectional height, *H*, and minimum cross-sectional height, *h*.

This increase in capsule dimensions is due to the uncompensated electrostatic repulsion between ionized carboxylic groups at pH = 7.4 observed earlier for PMAA films and spherical capsules.[54,61] We also found that the exposure of the discoidal (PMAA–PVPON) capsules to pH = 2 for several hours after core dissolution resulted in a dramatic change in the capsule shape. The confocal microscopy revealed the collapsed capsule interiors, which occurred most probably due to hydrogen bonding between PMAA and PVPON segments within the hydrogel walls and also through the capsule interior (Figure S3). Such behavior of the discoidal PMAA–PVPON hydrogel capsules under highly acidic conditions is because of the high aspect ratio of the discs and the small height (*H*) of the initial templates. However, the collapse was reversible. The capsules swelled at higher pH values (pH > 4) because of the hydrogel wall swelling due to ionization of PMAA segments. Strikingly, the $(PMAA)_{15}$ and $(PMAA-PVPON)_5$ capsules demonstrate various degrees of out-of-plane swelling of the discoidal circular faces (*i.e.*, circular face bulging) at pH = 7.4 (insets in Figure 2b and d and Figure 3).

To quantify the pH-triggered changes in aspect ratios of discoidal capsules, swelling behavior of the corresponding spherical capsules was studied. The spherical capsules were obtained using spherical silica templates (see Experimental Methods for details). Figure 4 shows $(PMAA)_{15}$ and $(PMAA-PVPON)_5$ spherical hydrogel capsules at pH = 4 and pH = 7.4. We found that the spherical $(PMAA)_{15}$ capsules displayed a dramatic 19-fold volume increase from 3.3 ± 0.2 μm^3 to 61.6 ± 3.8 μm^3 when solution pH was altered from

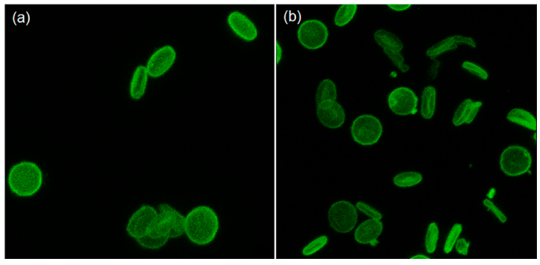

Figure 3. Three-dimensional reconstructions of confocal microscopy images of discoidal $(PMAA-PVPON)_5$ hydrogel capsules in their swollen (a) and deswollen (b) states in 0.01 M phosphate buffer solutions.

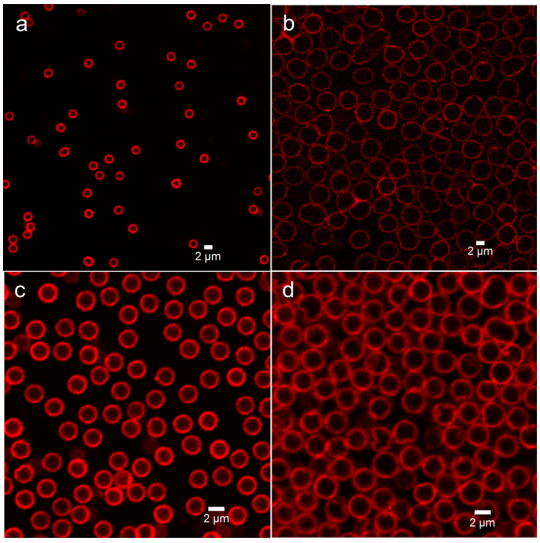

Figure 4. Confocal microscopy images of spherical $(PMAA)_{15}$ hydrogel capsules at pH = 4 (a) and pH = 7.4 (b) and spherical $(PMAA-PVPON)_5$ hydrogel capsules at pH = 4 (c) and at pH = 7.4 (d).

4 to 7.4. The capsule volume was calculated as $V = (4/3)\pi r^3$, where $r = L/2$ and *L* is the capsule diameter. These capsules increased in size from 1.84 ± 0.04 μm to 4.9 ± 0.1 μm upon the pH increase, indicating a 2.7-fold increase in capsule size (Figure 4a and b). This result is consistent with the previously shown several-fold change in diameters of cross-linked spherical PMAA capsules upon pH variations.[54,61] Unlike 19-fold swelling of $(PMAA)_{15}$ systems, two-component $(PMAA-PVPON)_5$ capsules undergo only a 2.9-fold increase in volume from 4.2 ± 0.3 μm^3 to 12.1 ± 0.8 μm^3 at pH = 4 and pH = 7.4, respectively, with capsule size changes from 2.00 ± 0.04 μm at pH = 4 to 2.85 ± 0.06 μm at pH = 7.4 (Figure 4c and d). This difference in pH-triggered variations in capsule size can be rationalized by comparing free volume within the capsule hydrogel shell. To estimate pH-triggered volume changes in the hydrogel wall, the thickness of $(PMAA)_5$ and $(PMAA-PVPON)_5$ hydrogel films attached to silicon wafers was measured with *in situ* ellipsometry (see Experimental Methods for details). As shown in Figure 5a, no swelling is observed for both

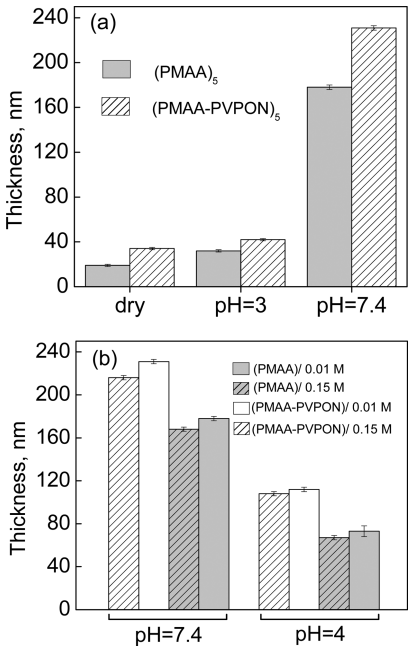

Figure 5. (a) Thicknesses of $(PMAA)_5$ and $(PMAA-PVPON)_5$ hydrogel films in their dry and wet states measured with *in situ* ellipsometry. (b) Thicknesses of the hydrogel films exposed to pH = 7.4 in 0.01 or 0.15 M phosphate buffers and being transferred to pH = 4 (0.01 or 0.15 M phosphate buffers) measured with *in situ* ellipsometry.

types of hydrogels at pH = 3, confirming the complete reaction of all amino groups during the cross-linking. Figure 5a shows that both types of hydrogels undergo a similar 5.5-fold change in thickness at pH variations from 3 to 7.4, consistent with the carboxylic group pK_a of ~5.6–7.[54] However, the $(PMAA)_5$ hydrogel displays a 2-fold greater water uptake than $(PMAA-PVPON)_5$ at pH = 3. Water contents of 41% and 19% are found for $(PMAA)_5$ and $(PMAA-PVPON)_5$, respectively (Figure 5a). Apparently, the presence of the second component reduces free volume in the dual-component network, suppressing capsule swelling. We also showed previously that the presence of PVPON increases shell rigidity, which results in a lower magnitude of size changes for two-component spherical capsules.[24] An additional parameter effecting rigidity in our case is a higher cross-link density in the two-component system. We found that there were, on average, 20 and 13 PMAA monomer units between the cross-links for $(PMAA)_{15}$ and $(PMAA-PVPON)_5$ hydrogels, respectively. The low cross-link density of PMAA in the single-component hydrogel permitted the release of PVPON from the network at pH = 8, as was previously confirmed by FTIR spectroscopy.[61,67] The cross-link densities for both types of hydrogel capsules were calculated using the molar ratios of the cross-linkable units within a copolymer chain obtained from ^1H NMR analysis of the PMAA-NH_2 or PVPON-NH_2 copolymers and their weight-average molecular weights. Thickness and pH-triggered volume changes of $(PMAA)_{15}$ and $(PMAA-PVPON)_5$ hydrogels

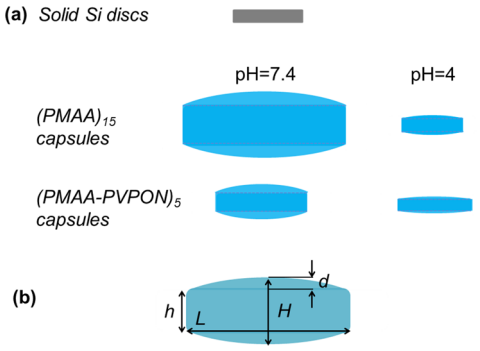

Figure 6. (a) Schematic presentations of solid cores and one- and two-component capsules at pH = 7.4 and pH = 4. (b) Dimensions of a bulged discoidal capsule including capsule diameter, *L*, maximum cross-sectional height, *H*, minimum cross-sectional height, *h*, and circular face deflection, *d*.

were not significantly affected by the presence of 0.15 M NaCl in solutions (Figure 5b).

Thus, spherical capsules exhibit uniform swelling (induced by the excess charge), resulting in their reversible isotropic swelling. We found in our previous study that PMAA–PVPON cubical capsules can swell uniformly, expanding in size upon pH variations.[61] Unlike spheres and cubes, where length (*L*) and height (*H*) are similar, discoidal capsules studied here have a higher aspect ratio of $L/H \gg 1$ (Figure 1a). In this aspect, the discoidal shape may be regarded as a derivative from the sphere with two circular faces of the initial sphere size, *L*, and the dramatically decreased height, *H*. Therefore, discoidal capsules might demonstrate a directional anisotropy in capsule swelling. For instance, the capsule volumes may preferentially increase in axial or radial directions, resulting in shape transformations. To quantify pH-triggered responses of $(PMAA)_{15}$ and $(PMAA-PVPON)_5$ discoidal capsules, capsule diameter, *L*, maximum cross-sectional height, *H*, minimum cross-sectional height, *h*, and circular face deflection, *d*, were found as shown in Figure 6 and inset in Figure 2d. These parameters at pH = 4 and pH = 7.4 are summarized in Table 1.

We found pH-triggered dimensional changes of $(PMAA)_{15}$ and $(PMAA-PVPON)_5$ discoidal capsules to be drastically different, as revealed in Table 1 and Figure 6. First, $(PMAA)_{15}$ showed a dramatic volume transition of 24-fold, while a moderate 2.3-fold volume change was found for $(PMAA-PVPON)_5$ capsules upon pH variations. The PMAA and PMAA–PVPON capsule volumes were calculated to be $38 \pm 10\ \mu m^3$ and $7 \pm 2\ \mu m^3$, respectively, at pH = 7.4 and $1.6 \pm 0.3\ \mu m^3$ and $3.1 \pm 0.6\ \mu m^3$, respectively, at pH = 4 (see Supporting Information). The observed reversible volume variations are consistent with those for the corresponding spherical systems. However, one-component discoidal capsules showed larger difference in volume variations (24-fold *vs* 19-fold for discoidal and spherical capsules, respectively).

TABLE 1. Capsule Size and Aspect Ratio Changes for $(PMAA)_{15}$ and $(PMAA-PVPON)_5$ Discoidal Hydrogel Capsules at pH = 4 and pH = 7.4, Where Subscripts i and f Stand for Initial (pH = 4) and Final (pH = 7.4) Capsule Dimensions, Respectively

	pH = 4	pH = 7.4
	$(PMAA)_{15}$ Discoidal Capsules	
h	0.33 ± 0.04 μm	1.02 ± 0.06 μm
L	2.33 ± 0.07 μm	6.4 ± 0.5 μm
H	0.67 ± 0.08 μm	2.23 ± 0.3 μm
h_f/h_i	3.1 ± 0.2	
L_f/L_i	2.7 ± 0.3	
L/H	3.5 ± 0.3	2.8 ± 0.3
	$(PMAA-PVPON)_5$ Discoidal Capsules	
h	0.44 ± 0.06 μm	0.59 ± 0.10 μm
L	2.95 ± 0.09 μm	3.6 ± 0.3 μm
H	0.58 ± 0.10 μm	1.2 ± 0.2 μm
h_f/h_i	1.34 ± 0.05	
L_f/L_i	1.22 ± 0.07	
L/H	5.2 ± 0.7	3.0 ± 0.3

Second, both radial (L) and axial (H) dimensions of PMAA capsules are 1.8-fold greater than those for PMAA−PVPON capsules at pH = 7.4. The larger expansion of the one-component hydrogel discs is consistent with the greater swelling of the corresponding hydrogel spheres and surface-attached hydrogel films as compared to their dual-component counterparts (Figures 2 and 6). However, the aspect ratios of two types of discoidal capsules, L/H, at pH = 7.4 remain similar, being 2.8 ± 0.3 and 3.0 ± 0.3 for PMAA and PMAA−PVPON, respectively, indicating that both types of hydrogels expand in a similar way in the ionized form. Note that these values are smaller than the aspect ratio of 5.6 (2.68 ± 0.07/0.45 ± 0.08) found for their solid templates, indicating the preferential expansion in the axial direction for both types of capsules upon core dissolution and exposure to neutral pH.

Another interesting aspect is that pH-triggered change in capsule dimensions results in anisotropic swelling/shrinkage, resulting in discoidal-to-ellipsoidal shape transformations. The degree of this shape transition depends on the wall composition (Figure 6). The PMAA capsules showed a 1.3-fold increase in aspect ratio (from 2.8 ± 0.3 to 3.5 ± 0.3) upon a pH change from pH = 7.4 to pH = 4. The PMAA−PVPON system displays a 1.7-fold increase (from 3.0 ± 0.3 to 5.2 ± 0.7) under the same conditions (Table 1). In this case, the aspect ratio of PMAA discoidal capsules (3.5 ± 0.3) was smaller than that for the PMAA−PVPON system (5.2 ± 0.7) at pH = 4. The results show that a one-component system undergoes greater change in radial direction than do two-component capsules. Indeed, the PMAA and PMAA−PVPON capsules showed decreases in radial dimensions of 2.7-fold (from 6.4 ± 0.5 to 2.33 ± 0.07 μm) and 1.2-fold (3.6 ± 0.3 to 2.95 ± 0.09 μm), respectively, when the pH was changed from 7.4 to 4. These variations in pH-triggered aspect ratios can be explained by a greater degree of out-of-plane swelling of PMAA capsules compared to that of PVPON−PMAA systems at pH = 7.4. To quantify the degree of swelling in axial and radial directions, the ratios of h_f/h_i and L_f/L_i were found, where subscripts i and f stand for initial (pH = 4) and final (pH = 7.4) capsule dimensions, respectively (Table 1). We found a negligible difference between h_f/h_i and L_f/L_i for both types of discoidal capsules, which implied no preferential swelling in axial or radial directions upon pH variations. The ratios h_f/h_i and L_f/L_i were 3.1 ± 0.2 *vs* 2.7 ± 0.3 for $(PMAA)_{15}$ and 1.34 ± 0.05 *vs* 1.22 ± 0.07 for $(PMAA-PVPON)_5$ capsules, respectively (Table 1).

Our overall results indicate that both types of capsules undergo pH-induced volume transitions with much greater volume changes for one-component systems. These changes were quantified through measuring variations in axial (h), radial (L), and out-of-plane ($H-h=d$) directions. The results show that both types of capsules exhibit shape transitions from discoids to oblate ellipsoids ($a = b > c$) due to the out-of-plane swelling, where a, b, and c are semiaxis lengths. These pH-triggered transitions are more pronounced for the single-component system, which shows 3-fold greater swelling/shrinkage in radial dimensions that that for the two-component capsules. The greater bulging of circular faces in PMAA discoid capsules is consistent with our previous observations on cubical capsules. In that work, cubical $(PMAA)_{20}$ capsules became bulged into spherical-like after exposure to neutral pH,[60] unlike more rigid $(PMAA-PVPON)_5$ cubes, which increased in size without bulging.[61] In our present study we observe that both types of capsules undergo pH-induced transitions from discs to ellipsoids probably due to the initially high aspect ratio of the discoidal geometry. At the same time, the degree of these transitions is controlled by the hydrogel rigidity through the chain stiffness similar to the cubical systems studied previously.[61] Indeed, more rigid PMAA−PVPON walls suppress an overall change in capsule dimensions, especially in the radial direction (Figure 6).

Interactions of Discoidal Hydrogel Capsules with Cells. The shape of the particulates as well as the nature of the blood vessels has an important role in interaction with the vasculature such as in the case of nonspherical filomicelles, which have been recently reported to show a prolonged circulation.[68] Interactions of spherical and discoidal $(PMAA-PVPON)_5$ capsules with three different cell lines including macrophage cells (J744.A1), human microvascular endothelial cells (HMVEC), and breast cancer cells (4T1) were explored. The results were compared with the internalization of corresponding solid templates (cores) including silica spheres and silicon discs. The choice of the cells was determined by their intrinsic characteristics pertaining to the uptake of particulates circulating in the bloodstream.

Indeed, the particulate introduced into the systemic circulation first encounters the endothelial cells lining the walls of the blood vessels and macrophages, which are the first to interact with foreign objects in the bloodstream. The 4T1 breast cancer cells were tested as one of the target populations for delivery vehicles that would carry a therapeutic cargo. Figure 7 demonstrates a representative image of three-dimensional reconstructions of consecutive focal plane confocal microscopy images of 4T1 cells incubated for 24 h with spherical (Figure 7a and b) and discoidal (Figure 7c and d) cores (left column) and the corresponding $(PMAA-PVPON)_5$ hydrogel capsules (right column) with the orthogonal (side panel) views. The cores were coated with a five-bilayer PMAA−PVPON hydrogel labeled with Alexa Fluor 568 (see Experimental Methods) for visualization. Cell nuclei and cytoskeleton appear in blue (DAPI) and green (Phalloidin 488), respectively. As seen from the side views, both cores and capsules were internalized by the cells. The quantitative analysis of cell association/internalization was carried out using confocal microscopy images by assessing at least 100 cells for each type of particle, and the number of associated/internalized particles was further normalized to the number of cells (Figures 8, 9, and S4).

We found that there was no significant difference in the internalization of solid discs by J774A.1 macrophages compared to solid spheres after 2 h of incubation (Figure 9a). The average number of spherical particles associated by the cells decreased 4-fold from 0.97 ± 0.05 to 0.24 ± 0.04 when spherical elastic capsules were incubated with the cells instead of solid spheres (Figure 9a). When solid and hydrogel discoidal particles were compared, we observed a 7.6-fold decrease in the particle-to-macrophage association from 1.15 ± 0.22 to 0.15 ± 0.05 particle per cell for solid discs and capsules, respectively. In both cases, hydrogel capsules were seen mainly as patches on the macrophage cell membrane with a negligible uptake by the J774A.1 macrophages (Figure 8). In addition, we found cellular association/internalization of the hydrogel capsules by the macrophages to be relatively slow (within several hours), unlike fast (within several minutes) uptake typically observed with solid particles.[69]

A similar trend of a lesser cellular association/internalization of soft hydrogel capsules in contrast to the solid cores was observed in the case of HMVEC endothelial and 4T1 breast cancer cells (Figure 9b and c). The numbers of particles associated/internalized per HMVEC endothelial cell after 24 h of incubation decreased from 1.48 ± 0.22 to 0.37 ± 0.04 and from 3.43 ± 0.79 to 0.22 ± 0.07 for spherical and discoidal systems, respectively (Figure 9b). The internalized discoidal cores and hydrogel capsules were found in the perinuclear region of HMVEC cells, while spherical cores had a more random distribution in the cytoplasm (Figure 8). 4T1 breast cancer cells also showed a 3.6-fold decrease in uptake of spherical capsules as compared to the spherical cores (Figure 9c). This difference in particle−4T1 cell interactions was more pronounced for discoidal systems, showing 0.6 ± 0.1 and 0.05 ± 0.01 particle per cell for core and capsules, respectively (Figure 9c). At the same time, the breast cancer cells clearly revealed more preferential uptake (5-fold) of spherical capsules as compared to discoidal ones (Figure 9b and d). Internalization of 2.5 particles per cell was reported for 600−800 nm thiolated PMAA spherical capsules incubated with colorectal cancer cells at the ratio of 100−600 particles/cell.[70] In our case we used the physiologically relevant 5:1 particle-to-cell ratio in the cell interaction experiments. This ratio could potentially be present at the same point of time following the intravenous administration of particles, while the larger ratios are statistically less possible in *in vivo* conditions in the body.

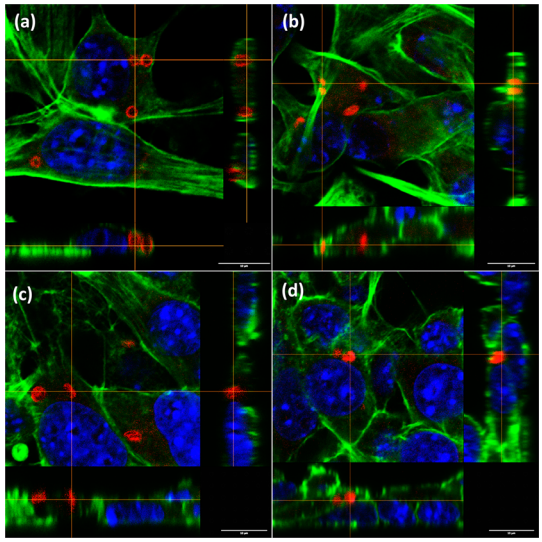

Figure 7. Three-dimensional reconstructions of consecutive focal plane confocal microscopy images of 4T1 cells incubated for 24 h with spherical (a, b) and discoidal (c, d) cores (a, c) and the corresponding $(PMAA-PVPON)_5$ hydrogel capsules (b, d) with their orthogonal (side panel) views. Particles are labeled red with Alexa Fluor 568. Cell nuclei and cytoskeleton appear in blue (DAPI) and green (Phalloidin 488), respectively. Scale bar is 10 μm in all images.

Our results demonstrate that hydrogel particles were internalized to a lesser extent compared to their solid counterparts. One of the reasons for such behavior is the significant difference in particle rigidity. As reported previously, the soft and flexible nature of worm-like micelles minimized phagocytosis and prolonged circulation of the micelles in the blood.[17] In another study, the uptake of hydrogel capsules was similar to the solid spheres, which was explained by their different entry pathways.[71] Another parameter that might affect capsule internalization is particle size.[71]

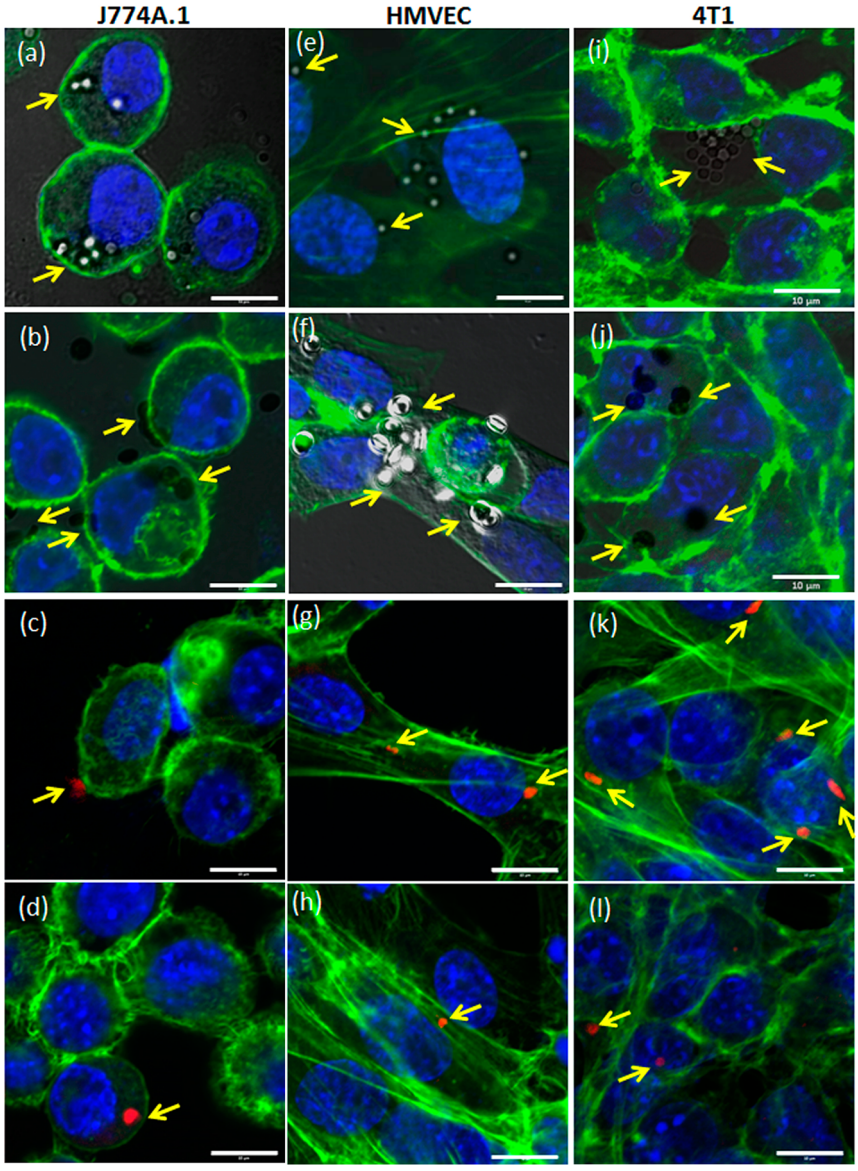

Figure 8. Confocal images of J774A.1 macrophages, HMVEC endothelial cells, and 4T1 cancer cells after incubation with spherical (a, e, i) or discoidal cores (b, f, j) and $(PMAA-PVPON)_5$ spherical (c, g, k) or discoidal shells (d, h, l) for 24 h, respectively. Arrows point to the particles associated with the cells. Cores were imaged using transmitted light, while shells are labeled red with Alexa Fluor 568. Cell nuclei and cytoskeleton appear in blue (DAPI) and green (Phalloidin 488), respectively. Scale bar is 10 μm in all images.

For instance, the *in vivo* uptake of the polymeric nanocarriers targeted to ICAM-1 was faster for small carriers with diameters of ≤ 5 μm compared to that of larger vehicles of 10−50 μm in diameter,[72] similarly to the results reported previously by two of us.[73] We observed that both spherical and discoidal capsules had an increased size of 4 μm under conditions of incubation, unlike unchanged dimensions of 2 μm solid spherical and discoidal cores. Our results also indicate that the cell interaction in the case of the discoidal capsules was persistently 60% lower than that for the spherical capsules (Figure 9d). The effect of the discoidal capsule shape on the cell interaction is clearly seen with 4T1 cells when the cellular internalization is 5-fold smaller ($p \leq 0.05$) for the discoidal hydrogel capsules compared to that of spherical ones (Figure 9d). This observation correlates well with the earlier studies on polystyrene particles, which showed that discs had decreased cellular uptake and had stronger cell surface binding as compared to spheres.[74] In another relevant study, disulfide-bonded PMAA hydrogel capsules of higher aspect ratio such as rod-shaped ones were internalized by cancer cells to a lower extent compared to the spherical capsules.[49] Our results also show that 4T1 breast cancer cells showed less cellular association of either cores or hydrogel capsules as compared to J774A.1 and HMVEC cells. Since 4T1 breast cells are of epithelial origin, they are not professional phagocytes in contrast to J774A.1 macrophage and HMVEC endothelial cell lines, resulting in less pronounced particle uptake by these cells.

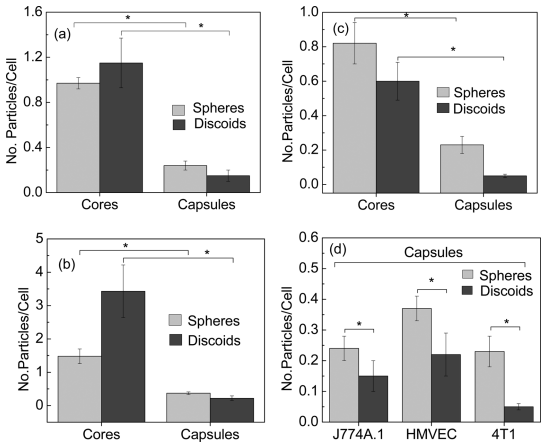

Figure 9. Average numbers of spherical (light gray) and discoidal (dark gray) rigid cores or soft $(PMAA-PVPON)_5$ capsules associated/internalized with (a) J774A.1, (b) HMVEC, and (c) 4T1 cells (*$p \leq 0.01$). (d) Association of spherical and discoidal $(PMAA-PVPON)_5$ hydrogel capsules with J774A.1, HMVEC, and 4T1 cells (*$p \leq 0.05$).

Finally, we discovered that hydrogel capsules significantly decreased in size upon internalization. Such a decrease in capsule size can occur due to either (i) local pH decrease or (ii) increased ionic strength. The intracellular ionic strength for most mammalian cells is around 155−160 mM[75] and can be higher (~200 mM) for red blood cells.[76] Multivalent ions such as Ca^{2+} and Mg^{2+} are reported to be present intracellularly in negligible concentrations of ~1 mM, with most of those in complexed states. Thus, based on our ellipsometry measurements of the hydrogel shrinkage at pH = 7.4 or pH = 4 in the presence of 0.15 M NaCl (Figure 5b), the swelling of the PMAA−PVPON hydrogel wall is decreased by only 6% due to salt screening. At pH = 4, the PMAA−PVPON hydrogel wall swelling is suppressed by the high ionic strength of 0.15 M by only 8%, which is similar to that observed at pH = 7.4. Apparently, the capsule size decrease is because of the intracellular local decrease in pH. This remarkable observation can provide information on the microenvironment of the internalized capsules and could be used for controlled intracellular release of cargo from the capsule interior. As known, the endosomal internalization pathway is associated with changes in the pH of the particles' environment from the physiological values of pH = 7.2−7.4 to acidic pH values in the early endosomes of pH = 5−6.5.[77] We found that spherical and discoidal capsules demonstrated a 2-fold decrease in size upon internalization by HMVECs and 4T1 cells. After internalization by the HMVECs, the diameters of the spherical and discoidal capsules were reduced from 4.0 ± 0.5 μm to 2.8 ± 0.8 μm and from 4.0 ± 0.3 μm to 1.7 ± 0.8 μm, respectively. Internalization by 4T1 cells led to the reduction in the capsule size from 4.0 ± 0.5 μm to 2.1 ± 0.5 μm and from 4.0 ± 0.3 μm to 2.4 ± 0.4 μm of the spherical and discoidal capsules, respectively. Previous *in vitro* studies on phagocytic cells demonstrated that macrophages internalized IgG-coated polystyrene spherical particles of 0.2−2 μm through different intracellular delivery pathways.[78,79] While nanospheres were taken up by clathrin-mediated endocytosis, the microspheres undergo classical phagocytosis, trafficking more rapidly to the lysosomes. In a recent study, internalization of polyelectrolyte multilayer capsules was found to occur as a sequence of different mechanisms, leading to formation of very acidic internalization vesicles co-localized with lysosome markers.[80] Endocytic pathways for particulates in endothelial cells generally include phagocytosis, clathrin- or calveoli-mediated uptake, macropinocytosis, receptor-mediated endocytosis, or cell adhesion molecule-mediated endocytosis.[81] In our case, following internalization, the hydrogel capsule decreased in size 2-fold due to the increased acidity in the cell organelle environment. Accounting for the microscopic sizes of these particles, they should undergo endocytosis associated with shifts in the intracellular pH. As reported previously, particle uptake can be significantly reduced in endothelial cells under chronic shear stress due to the formation of actin stress fibers, and a similar scenario was witnessed in the case of arterial endothelial cells, *in vivo*.[82] On the other hand, the absence of actin stress fibers in endothelial cells grown under an acute stress environment resulted in enhanced particle uptake *in vivo*.[82] Thus, the evaluation of the cellular uptake of the pH-sensitive shape-responsive capsules in the endothelial cell cultures under hydrodynamic conditions will have to be performed in parallel to *in vivo* evaluation of the systems for more insights on the influence of the carrier geometry on cell internalization.

CONCLUSIONS

We report on synthesis and cellular uptake of discoidal hydrogel capsules of cross-linked PMAA capable of drastic and reversible volume transitions and aspect ratios upon pH variations. The capsules were fabricated by LbL template synthesis using sacrificial silicon templates of discoidal geometry. The pH-triggered change in capsule volume resulted in anisotropic out-of-plane swelling, leading to the discoidal-to-ellipsoidal shape transformations. The degree of this shape transition was controlled by the pH-tuned volume change, which in turn was regulated by the capsule wall composition. We showed that $(PMAA)_{15}$ capsules underwent a dramatic 24-fold volume change, while a moderate 2.3-fold volume variation was observed for $(PVPON-PMAA)_5$ capsules when solution pH transitioned from pH = 7.4 to pH = 4. Those volume variations were consistent with those for the corresponding spherical systems. We also observed a 3-fold greater swelling/shrinkage in radial dimensions for one-component capsules than that for the two-component capsules. The aspect ratios were found to increase from 2.8 ± 0.3 to 3.5 ± 0.3 for $(PMAA)_{15}$ and from 3.0 ± 0.3 to

5.2 ± 0.7 for (PMAA−PVPON)$_5$ discoidal capsules, respectively, when the pH changed from neutral low. These differences in aspect ratios were due to a greater degree of the circular face bulging for PMAA capsules compared to that for PMAA−PVPON capsules. The interaction of (PMAA−PVPON)$_5$ hydrogel capsules with cells was studied using J774A.1 macrophage, HMVEC endothelial, and 4T1 breast cancer cells. We showed that hydrogel capsules exhibited lower association/internalization by the macrophage cells in contrast to their rigid counterparts. The discoidal shape of the hydrogel capsules was demonstrated to inhibit the interactions with the studied type of cells, indicating their potential for prolonged circulation. Finally, we found that spherical and discoidal capsules demonstrated a 2-fold decrease in dimensions upon internalization by HMVECs and 4T1 cells. Our results illustrate that hydrogel capsules are versatile platforms for developing hydrogel microstructures with pH-controlled shapes and sizes. The demonstrated approach is simple and robust and integrates advantages of discoidal shape and pH-sensitivity to develop novel types of shape-specific "intelligent" networks with programmable behavior to be potentially used for delivery of functional cargo. In the current study, we have evaluated *in vitro* behavior of hollow pH-responsive hydrogel particles with dimensions and geometry resembling those of the circulating cells. The association of the hydrogel hollow replicas with macrophages was reduced 5-fold as compared to the rigid templates. Studies on the behavior of the deformable hydrogel capsules under flow and in animal models to understand the therapeutic potential of these systems are currently under way. The ability to alter dimensions in response to environmental pH variations may be further explored for shape-regulated transport and cellular uptake.

EXPERIMENTAL METHODS

Materials. Poly(*N*-vinylpyrrolidone) (average M_w 55 000 g mol^{-1}), poly(methacrylic acid) (PMAA, average M_w 100 000 g mol^{-1}), poly(ethylene imine) (PEI, average M_w 25 000 g mol^{-1}), 1-ethyl-3-(3-(dimethylamino)propyl)carbodiimide hydrochloride (EDC), and *N*-vinylpyrrolidone (VPON) were obtained from Sigma-Aldrich. *tert*-Butyl methacrylate (*t*BMA), *N*-(*tert*-butoxycarbonyl-aminopropyl)methacrylamide (*t*BOC), and monodisperse silica microspheres of 2 μm were from Polysciences, Inc. Alexa Fluor 488 carboxylic acid, succinimidyl ester (Ex/Em = 488/510 nm), and Alexa Fluor 488 dihydrazide sodium salt were purchased from Invitrogen. 2,2′-Azobis(2-methylpropionitrile) (AIBN) was purchased from Sigma-Aldrich and recrystallized from methanol at 30 °C before use. Ultrapure deionized water with a resistivity of 0.055 μS/cm was used in all experiments (Siemens). NaH_2PO_4 and Na_2HPO_4 (Sigma-Aldrich) of ACS grade were used. 1,4-Dioxane, diethyl ether, hexane, and methanol were purchased from Fisher Scientific and used as received.

Copolymer Synthesis. Amino-containing poly(*N*-vinylpyrrolidone) or poly(methacrylic acid) copolymers, PVPON-NH_2-*n* and PMAA-NH_2-*m*, respectively, with *n* and *m* representing molar percentage of amino-group-containing polymer units, were synthesized using copolymerization of VPON and *t*BOC for PVPON-NH_2 or by copolymerization of *tert*-butyl acrylate with *t*BOC in the presence of AIBN for PMAA-NH_2 as described in our previous work.[61] The molecular weights of PVPON-NH_2-7 (M_w = 143 884 g mol^{-1}, M_w/M_n =1.55) and PMAA-NH_2-5 (M_w = 130 000, M_w/M_n =1.50) were determined with GPC (Waters) using linear poly(vinylpyrrolidone) (American Polymer Standards Corp.) or polystyrene (Waters) standards, respectively.

Fabrication of Silicon Discs. The discoidal nonporous silicon particles were fabricated from polycrystalline silicon (PolySi) film by photolithography with a reactive ion etching of silicon. Briefly, starting with a silicon wafer, a 500 nm silicon dioxide (SiO_2) film was deposited by using a furnace-based wet oxidation process. A PolySi layer of the desired thickness (400 nm) was then deposited by low-pressure chemical vapor deposition, followed by a deposition of a 100 nm SiO_2 film using a thermal oxidation process. Arrays of 2.6 μm circles were patterned all over the wafer using a standard photolithography process. A CF_4 reactive ion etch (RIE) was applied to remove the undesired area of the SiO_2 film; then PolySi particles were formed by RIE of the PolySi layer (Plasmatherm 790 series, 4 sccm Cl_2 25.4 sccm HBr, 150 mTorr, 250 W rf power). The particles were detached from the substrate by selective removal of the box oxide layer in diluted hydrofluoric (HF) acid solution and collected in 2-propanol.

Capsule Preparation. For all deposition steps, 0.5 mg mL^{-1} polymer solutions were used with a 10 min deposition time. Hydrogen-bonded multilayers of (PMAA-NH_2-5/PVPON)$_n$ or (PMAA/PVPON-NH_2-7)$_n$ where the subscript denotes the number of polymer bilayers, were deposited on the silica microspheres or silicon discs. A layer of PEI was allowed to adsorb first from a 0.5 mg mL^{-1} aqueous solution at pH = 6. Assembly of the hydrogen-bonded layers was then performed at pH = 2.6, starting from PMAA. Each deposition cycle was followed by three rinsing steps at pH = 2.6 (0.01 M NaH_2PO_4) to remove excess polymer, followed by centrifugation of suspensions at 5000 rpm for 2 min to remove supernatant. After a desired number of layers were deposited, chemical cross-linking of PMAA-NH_2 or PMAA/PVPON-NH_2 layers was performed. For that, the core−shell particles were exposed to the carbodiimide solution (5 mg mL^{-1}) at pH = 5 for 60 min, followed by 3 h of shaking at pH = 6 (0.01 M NaH_2PO_4). After that, coated microparticles were exposed to pH = 8 (0.01 M NaH_2PO_4) for 6 h, followed by several washings at pH = 4 (0.01 M NaH_2PO_4). The silica and silicon discoid cores were dissolved in an 8% aqueous solution of hydrofluoric acid and in HF/NHO_3, 3:1 v/v, respectively, followed by dialysis in aqueous solution at pH = 4 using Float-A-lyzer tubes (Spectrum Laboratories) with an MWCO of 20 000 g mol^{-1} for 2 days. For the (PMAA-NH_2-5/PVPON)$_n$ or (PMAA/PVPON-NH_2-7)$_n$ multilayer assembly on planar supports, the hydrogen-bonded films were dipped-coated onto silicon wafers (1 cm × 2 cm). A layer of poly(glycidyl methacrylate) was covalently bound to the silica surface of a Si wafer followed by deposition of PEI as described previously.[51] The assembly of the films was performed from 0.5 mg mL^{-1} solutions at pH = 2.6 with a deposition time of 10 min. After depositing a desired number of polymer bilayers, the films were cross-linked as described for capsules.

Cell Internalization. Murine macrophage J774A.1 and breast cancer 4T1 cells (American Type Culture Collection, USA) and human microvascular endothelial cells (HMVEC, Lonza Walkersville Inc., USA) were cultured in DMEM (J774A.1) or in MEM (4T1) supplemented with 10% fetal bovine serum and 1% penicillin−streptomycin (Gibco, Life Technologies, USA) and in endothelial basal medium (HMVEC) supplemented with SingleQuot growth factors, cytokines, and supplements (EGM-MV BulletKit, Lonza Walkersville Inc., USA). HMVEC and 4T1 cells were seeded in an eight-well chambered cover-glass (BD Biosciences, USA) at 37 °C overnight at a population of 25 000 cells per well, and at 50 000 cells per well for J774A.1 cells. Particles were added at a particle-to-cell ratio of 5:1 in each well. After a certain period of time (2−24 h), the cells were washed with PBS containing $CaCl_2$ and $MgCl_2$ three times to remove free-floating particles

and fixed with methanol-free 4% paraformaldehyde at room temperature for 15 min. For confocal microscopy analysis, the cells were washed, permeabilized with 0.1% Triton X-100 (Sigma-Aldrich, MO, USA) for 5 min, incubated with Alexa Fluor 488 phalloidin (Molecular Probes, USA) for 30 min to stain the cytoskeleton of cells, and washed three times. The slides were sealed with coverslips using ProLong Gold antifade reagent with DAPI (Molecular Probes, USA). The mounted slides were allowed to dry and sealed by applying Richard-Allan Scientific Cytoseal XYL (Thermo Scientific, USA) along the edges of the slide.

Analytical Methods. Scanning electron microscopy (SEM) was performed using a FEI Quanta FEG microscope at 10 kV. Samples were prepared by placing a drop of a particle suspension on a silicon wafer and allowing it to dry at room temperature. Before imaging, dried specimens were sputter-coated with approximately 5 nm silver film using a Denton sputter-coater. Film thickness measurements were performed using a M2000U spectroscopic ellipsometer (J.A. Woollam). Silicon wafers were cut into 1 cm × 2 cm substrates and cleaned by immersion in piranha solution (H_2SO_2/H_2O_2 (1:3, v/v)) for 1 h (*Caution: Piranha solution is highly corrosive and reacts violently with organic matter!*) Prior to use, substrates were rinsed with deionized water, blow-dried with filtered nitrogen, and used immediately thereafter. Wafers containing cross-linked multilayers were exposed to pH = 8 for 24 h to remove poly(*N*-vinylpyrrolidone) from cross-linked PMAA-NH_2/PVPON films, transferred to pH = 4 to deswell the films, and dried. Dry measurements were performed between 400 and 1000 nm at 65°, 70°, and 75° angles of incidence. The ellipsometric angles, Ψ and Δ, were fitted using a multilayer model composed of silicon, silicon oxide, and the multilayer film to obtain the thickness of the films. The thickness of SiO_2 was measured for each wafer and was determined using known optical constants. The thickness of the multilayer film was obtained by fitting data with the Cauchy approximation. Studies of film swelling were performed using a 5 mL liquid flow-through cell (Woollam). Confocal images of capsules were obtained with Zeiss LSM 710 confocal microscope equipped with a 63× oil immersion objective. To observe pH-dependent changes, a drop of a hollow capsule dispersion was added to a chambered cover-glass filled with 0.01 M NaH_2PO_4 solutions at a certain pH value. Capsules were allowed to settle at the chamber bottom for 3 h and imaged.

Particle−Cell Interactions. The interactions of the cells with particles at various time points were captured with a Nikon A1 confocal imaging system. The 350/488/568 nm excitation filters were used, and images were captured using a 60× oil immersion objective. The images were analyzed using NIS Elements software (Nikon). Optical sections of 125 nm in thickness were analyzed to verify if the particles were internalized or associated with the cells. The length of the major axis of the particles internalized by the cells as well as of those not associated with the cells was measured from the captured images using NIS Elements. At least 100 cells were analyzed from the confocal microscopy images for each system, and the average numbers of particles associated with cells were obtained by counting the number of internalized particles per cell for each field. The mean and standard deviations of the particle dimensions measured were represented with at least six data entry points per group. For statistical analysis, Student's *t* test (two-tailed distribution, two-sample equal variance) was performed, and $p \leq 0.05$ values were considered statistically significant.

Conflict of Interest: The authors declare no competing financial interest.

Acknowledgment. This work was supported in part by NSF CAREER Award 1350370 (EK) and also performed pursuant to an agreement with Houston Methodist Research Institute supported by Grant Number U54 CA143837 from Cancer Institute (NCI), National NIH (EK and BG). BG, JA and XL also acknowledge the support from 1U54CA151668-01 from NCI, NIH. X. Liang (UAB) is acknowledged for GPC analysis of block copolymers. W. Higgins (UAB) is acknowledged for technical assistance.

Supporting Information Available: Calculations of hydrogel capsule volumes in their swollen and deswollen states, confocal images of $(PMAA-PVPON)_5$ discoidal capsules at pH = 2, and the percentage of J774A.1 macrophage, HMVEC endothelial, and 4T1 breast cancer cells associated with spherical and discoidal cores and capsules. This material is available free of charge *via* the Internet at http://pubs.acs.org.

REFERENCES AND NOTES

1. Gopal, V.; Kumar, A.; Usha, A.; Karthik, A.; Udupa, N. Effective Drug Targeting by Erythrocytes as Carrier Systems. *Curr. Trends Biotechnol. Pharm.* **2007**, *1*, 18–33.
2. Li, J.; Lykotrafitis, G.; Dao, M.; Suresh, S. Cytoskeletal Dynamics of Human Erythrocyte. *Proc. Natl. Acad. Sci. U.S.A.* **2007**, *104*, 4937–4942.
3. Diez-Silva, M.; Dao, M.; Han, J.; Lim, C.-T.; Suresh, S. Shape and Biomechanical Characteristics of Human Red Blood Cells in Health and Disease. *MRS Bull.* **2010**, *35*, 382–388.
4. Suresh, S. Nanomedicine: Elastic Clues in Cancer Detection. *Nat. Nanotechnol.* **2007**, *2*, 748–749.
5. Mitragotri, S.; Lahann, J. Physical Approaches to Biomaterial Design. *Nat. Mater.* **2009**, *8*, 15–23.
6. Elinav, E.; Peer, D. Harnessing Nanomedicine for Mucosal Theranostics - A Silver Bullet at Last? *ACS Nano* **2013**, *7*, 2883–2890.
7. Hamad, I.; Al-Hanbali, O.; Hunter, A. C.; Rutt, K. J.; Andresen, T. L.; Moghimi, S. M. Distinct Polymer Architecture Mediates Switching of Complement Activation Pathways at Nanosphere-Serum Interface: Implications for Stealth Nanoparticle Engineering. *ACS Nano* **2010**, *4*, 6629–6638.
8. Muzykantov, V. R. Drug Delivery Carriers on the Fringes: Natural Red Blood Cells *versus* Synthetic Multilayered Capsules. *Expert Opin. Drug Delivery* **2013**, *10*, 1–4.
9. Champion, J. A.; Katare, Y. K.; Mitragotri, S. Particle Shape: A New Design Parameter for Micro- and Nanoscale Drug Delivery Carriers. *J. Controlled Release* **2007**, *121*, 3–9.
10. Decuzzi, P.; Ferrari, M. The Receptor-Mediated Endocytosis of Nonspherical Particles. *Biophys. J.* **2008**, *94*, 3790–3797.
11. Meng, H.; Yang, S.; Li, Z.; Xia, T.; Chen, J.; Ji, Z.; Zhang, H.; Wang, X.; Lin, S.; Huang, C.; *et al*. Aspect Ratio Determines the Quantity of Mesoporous Silica Nanoparticle Uptake by a Small GTPase-Dependent Macropinocytosis Mechanism. *ACS Nano* **2011**, *5*, 4434–4447.
12. Wang, J.; Byrne, J. D.; Napier, M. E.; DeSimone, J. M. More Effective Nanomedicines through Particle Design. *Small* **2011**, *7*, 1919–1931.
13. Tao, L.; Hu, W.; Liu, Y.; Huang, G.; Sumer, B. D.; Gao, J. Shape-Specific Polymeric Nanomedicine: Emerging Opportunities and Challenges. *Exp. Biol. Med.* **2011**, *236*, 20–29.
14. Champion, J. A.; Mitragotri, S. Role of Target Geometry in Phagocytosis. *Proc. Natl. Acad. Sci. U.S.A.* **2006**, *103*, 4930–4934.
15. Ferrari, M. Nanogeometry: Beyond Drug Delivery. *Nat. Nanotechnol.* **2008**, *3*, 131–132.
16. Merkel, T.; Jones, S.; Herlihy, K.; Kersey, F.; Shields, A.; Napier, M.; Luft, J.; Wu, H.; Zamboni, W. C.; Wang, A. Z.; *et al*. Using Mechanobiological Mimicry of Red Blood Cells to Extend Circulation Times of Hydrogel Microparticles. *Proc. Natl. Acad. Sci. U.S.A.* **2011**, *108*, 586–591.
17. Geng, Y.; Dalheimer, P.; Cai, S.; Tsai, R.; Tewari, M.; Minko, T.; Discher, D. E. Shape Effects of Filaments *Versus* Spherical Particles in Flow and Drug Delivery. *Nat. Nanotechnol.* **2007**, *2*, 249–255.
18. Shah, S.; Liu, Y.; Hu, W.; Gao, J. Modeling Particle Shape-dependent Dynamics in Nanomedicine. *J. Nanosci. Nanotechnol.* **2011**, *11*, 919–928.
19. Gentile, F.; Chiappini, C.; Fine, D.; Bhavane, R. C.; Peluccio, M. S.; Cheng, M. M.-C.; Liu, X.; Ferrari, M.; Decuzzi, P. The Effect of Shape on the Margination Dynamics of Non-Neutrally Buoyant Particles in Two-Dimensional Shear Flows. *J. Biomech.* **2008**, *41*, 2312–2318.
20. Lee, S.- Y.; Ferrari, M.; Decuzzi, P. Shaping Nano-/Microparticles for Enhanced Vascular Interaction in Laminar Flows. *Nanotechnology* **2009**, *20*, 495101–495111.
21. Godin, B.; Chiappini, C.; Srinivasan, S.; Alexander, J. F.; Yokoi, K.; Ferrari, M.; Decuzzi, P.; Liu, X. Discoidal Porous

Silicon Particles: Fabrication and Biodistribution in Breast Cancer Bearing Mice. *Adv. Funct. Mater.* **2012**, *22*, 4225–4235.
22. Beningo, K.; Wang, Y. Fc-Receptor-Mediated Phagocytosis Is Regulated by Mechanical Properties of the Target. *J. Cell Sci.* **2002**, *115*, 849–856.
23. Liu, W.; Zhou, X.; Mao, Z.; Yu, D.; Wang, B.; Gao, C. Uptake of Hydrogel Particles with Different Stiffness and Its Influence on HepG2 Cell Functions. *Soft Matter* **2012**, *8*, 9235–9245.
24. Gao, G.; Donath, E.; Moya, S.; Dudnik, V.; Möhwald, H. Elasticity of Hollow Polyelectrolyte Capsules Prepared by the Layer-by-Layer Technique. *Eur. Phys. J. E* **2001**, *5*, 21–27.
25. Dubreuil, F.; Elsner, N.; Fery, A. Elastic Properties of Polyelectrolyte Capsules Studied by Atomic Force Microscopy and RICM. *Eur. Phys. J. E* **2003**, *12*, 215–221.
26. Vinogradova, O. I.; Andrienko, D.; Lulevich, V. V.; Nordschild, S.; Sukhorukov, G. B. Young's Modulus of Polyelectrolyte Multilayers from Microcapsule Swelling. *Macromolecules* **2004**, *37*, 1113–1117.
27. Elsner, N.; Kozlovskaya, V.; Sukhishvili, S. A.; Fery, A. pH-Triggered Softening of Crosslinked Hydrogen-Bonded Capsules. *Soft Matter* **2006**, *2*, 966–972.
28. Lisunova, M. O.; Drachuk, I.; Shchepelina, O. A.; Anderson, K. D.; Tsukruk, V. V. Direct Probing of Micromechanical Properties of Hydrogen-Bonded Layer-by-Layer Microcapsule Shells with Different Chemical Compositions. *Langmuir* **2011**, *27*, 11157–11165.
29. Chen, J.; Kozlovskaya, V.; Goins, A.; Campos-Gomez, J.; Saeed, M.; Kharlampieva, E. Biocompatible Shaped Particles from Dried Multilayer Polymer Capsules. *Biomacromolecules* **2013**, *14*, 3830–3841.
30. Such, G. K.; Johnston, A. P. R.; Caruso, F. Engineered Hydrogen-Bonded Polymer Multilayers: From Assembly to Biomedical Applications. *Chem. Soc. Rev.* **2011**, *40*, 19–29.
31. Shutava, T.; Prouty, M.; Kommireddy, D.; Lvov, Y. pH-Responsive Decomposable Layer-by-Layer Nanofilms and Capsules on the Basis of Tannic Acid. *Macromolecules* **2005**, *38*, 2850–2858.
32. Mauser, T.; Dejugnat, C.; Sukhorukov, G. B. Balance of Hydrophobic and Electrostatic Forces in the pH Response of Weak Polyelectrolyte Capsules. *J. Phys. Chem. B* **2006**, *110*, 20246–20253.
33. DeVilliers, M.; Lvov, Y. Layer-by-layer Self-Assembled Nanoshells for Drug Delivery. *Adv. Drug Delivery Rev.* **2011**, *63*, 699–701.
34. Kozlovskaya, V.; Ok, S.; Sousa, A.; Libera, M.; Sukhishvili, S. A. Hydrogen-Bonded Polymer Capsules Formed by Layer-by-Layer Self-assembly. *Macromolecules* **2003**, *36*, 8590–8592.
35. Hiller, J.; Rubner, M. F. Reversible Molecular Memory and pH-Switchable Swelling Transitions in Polyelectrolyte Multilayers. *Macromolecules* **2003**, *36*, 4078–4083.
36. Matsusaki, M.; Akashi, M. Functional Multilayered Capsules for Targeting and Local Drug Delivery. *Expert Opin. Drug Delivery* **2009**, *6*, 1207–1217.
37. Tong, W. J.; Gao, C. Y. Multilayer Microcapsules with Tailored Structures for Bio-related Applications. *J. Mater. Chem.* **2008**, *18*, 3799–3812.
38. Skirtach, A. G.; Yashchenok, A. M.; Möhwald, H. Encapsulation, Release and Applications of LbL Polyelectrolyte Multilayer Capsules. *Chem. Commun.* **2011**, *47*, 12736–12746.
39. Del Mercato, L. L.; Rivera-Gil, P.; Abbasi, A. Z.; Ochs, M.; Gnas, C.; Zins, I.; Sönnichsen, G.; Parak, W. J. LbL Multilayer Capsules: Recent Progress and Future Outlook for Their Use in Life Sciences. *Nanoscale* **2010**, *2*, 458–467.
40. Lvov, Y.; Decher, G.; Möhwald, H. Assembly, Structural Characterization and Thermal Behavior of Layer-by-Layer Deposited Ultrathin Films of Polyvinylsulfate and Polyallylamine. *Langmuir* **1993**, *9*, 481–486.
41. *Multilayer Thin Films: Sequential Assembly of Nanocomposite Materials*; Decher, G.; Schlenoff, J. B., Eds.; Wiley-VCH: Weinheim, 2002.
42. Tang, Z.; Wang, Y.; Podsiadlo, P.; Kotov, N. A. Biomedical Applications of Layer-by-Layer Assembly: From Biomimetics to Tissue Engineering. *Adv. Mater.* **2006**, *18*, 3203–3224.
43. Ghostine, R. A.; Markarian, M. Z.; Schlenoff, J. B. Asymmetric Growth in Polyelectrolyte Multilayers. *J. Am. Chem. Soc.* **2013**, *135*, 7636–7646.
44. Morton, S. W.; Poon, Z.; Hammond, P. T. The Architecture and Biological Performance of LbL Nanoparticles. *Biomaterials* **2013**, *34*, 5328–5335.
45. Holt, B.; Lam, R.; Meldrum, F. C.; Stoyanov, S. D.; Paunov, V. N. Anisotropic Nano-Papier Mache Microcapsules. *Soft Matter* **2007**, *3*, 188–190.
46. Donath, E.; Moya, S.; Neu, B.; Sukhorukov, G. B.; Georgieva, R.; Voigt, A.; Baumler, H.; Kiesewetter, H.; Mohwald, H. Hollow Polymer Shells from Biological Templates: Fabrication and Potential Applications. *Chem.—Eur. J.* **2002**, *8*, 5481–5485.
47. Yashchenok, A.; Parakhonskiy, B.; Donatan, S.; Kohler, D.; Skirtach, A.; Möhwald, H. Polyelectrolyte Multilayer Microcapsules Templated on Spherical, Elliptical and Square Calcium Carbonate Particles. *J. Mater. Chem. B* **2013**, *1*, 1223–1228.
48. Shchepelina, O.; Kozlovskaya, V.; Kharlampieva, E.; Mao, W.; Alexeev, A.; Tsukruk, V. V. Anisotropic Micro- and Nanocapsules. *Macromol. Rapid Commun.* **2010**, *31*, 2041–2046.
49. Shimoni, O.; Yan, Y.; Wang, Y.; Caruso, F. Shape-Dependent Cellular Processing of Polyelectrolyte Capsules. *ACS Nano* **2013**, *7*, 522–530.
50. Kozlovskaya, V.; Baggett, J.; Godin, B.; Liu, X.; Kharlampieva, E. Hydrogen-Bonded Multilayers of Silk Fibroin: From Coatings to Cell-Mimicking Shaped Microcontainers. *ACS Macro Lett.* **2012**, *1*, 384–387.
51. Liang, X.; Kozlovskaya, V.; Chen, Y.; Zavgorodnya, O.; Kharlampieva, E. Thermosensitive Multilayer Hydrogels of Poly(N-vinylcaprolactam) as Nanothin Films and Shaped Capsules. *Chem. Mater.* **2012**, *24*, 3707–3719.
52. Yang, S. Y.; Rubner, M. F. Micropatterning of Polymer Thin Films with pH-Sensitive and Cross-Linkable Hydrogen-Bonded Polyelectrolyte Multilayers. *J. Am. Chem. Soc.* **2002**, *124*, 2100–2101.
53. Lee, D.; Rubner, M. F.; Cohen, R. E. Formation of Nanoparticle-Loaded Microcapsules Based on Hydrogen-Bonded Multilayers. *Chem. Mater.* **2005**, *17*, 1099–1105.
54. Kozlovskaya, V.; Kharlampieva, E.; Mansfield, M. L.; Sukhishvili, S. A. Poly(methacrylic acid) Hydrogel Films and Capsules: Response to pH and Ionic Strength, and Encapsulation of Macromolecules. *Chem. Mater.* **2006**, *18*, 328–336.
55. Zelikin, A. N.; Li, Q.; Caruso, F. Disulfide-Stabilized Poly(methacrylic acid) Capsules: Formation, Cross-Linking, and Degradation Behaviour. *Chem. Mater.* **2008**, *20*, 2655–2661.
56. She, S.; Li, Q.; Shan, B.; Tong, W.; Gao, C. Fabrication of Red-Blood-Cell-Like Polyelectrolyte Microcapsules and Their Deformation and Recovery Behaviour through a Microcapillary. *Adv. Mater.* **2013**, *25*, 5814–5818.
57. Chong, S.-F.; Lee, J. H.; Zelikin, A. N.; Caruso, F. Tuning the Permeability of Polymer Hydrogel Capsules: An Investigation of Crosslinking Density, Membrane Thickness, and Cross-Linkers. *Langmuir* **2011**, *27*, 1724–1730.
58. Sivakumar, S.; Bansal, V.; Cortez, C.; Chong, S. F.; Zelikin, A. N.; Caruso, F. Degradable, Surfactant-Free, Monodisperse Polymer-Encapsulated Emulsions as Anticancer Drug Carriers. *Adv. Mater.* **2009**, *21*, 1820–1824.
59. Chong, S. F.; Sexton, A.; De Rose, R.; Kent, S. J.; Zelikin, A. N.; Caruso, F. A Paradigm for Peptide Vaccine Delivery Using Viral Epitopes Encapsulated in Degradable Polymer Hydrogel Capsules. *Biomaterials* **2009**, *30*, 5178–5186.
60. Kozlovskaya, V.; Higgins, W.; Chen, J.; Kharlampieva, E. Switching Shape of Layer-By-Layer Hydrogel Microcontainers. *Chem. Commun.* **2011**, *47*, 8352–8354.
61. Kozlovskaya, V.; Wang, Y.; Higgins, W.; Chen, J.; Chen, Y.; Kharlampieva, E. pH-Triggered Shape Response of Cubical Ultrathin Hydrogel Capsules. *Soft Matter* **2012**, *8*, 9828–9839.
62. Chen, G.-T.; Wang, C.-H.; Zhang, J.-G.; Wang, Y.; Zhang, R.; Du, F.-S.; Yan, N.; Kou, Y.; Li, Z.-C. Toward Functionalization of Thermoresponsive Poly(N-vinyl-2-pyrrolidone). *Macromolecules* **2010**, *43*, 9972–9981.

63. Tardajos, M. G.; Nash, M.; Rochev, Y.; Reinecke, H.; Elvira, C.; Gallardo, A. Homologous Copolymerization Route to Functional and Biocompatible Polyvinylpyrrolidone. *Macromol. Chem. Phys.* **2012**, *213*, 529–538.
64. Andersen, T. E.; Palarasah, Y.; Skjødt, M. O.; Ogaki, R.; Benter, M.; Alei, M.; Kolmos, H. J.; Koch, C.; Kingshott, P. Decreased Material-Activation of the Complement System Using Low-Energy Plasma Polymerized Poly(vinyl pyrrolidone) Coatings. *Biomaterials* **2011**, *32*, 4481–4488.
65. Gaucher, G.; Asahina, A.; Wang, J.; Leroux, J. C. Effect of Poly(N-vinyl-pyrrolidone)-block-poly(d,l-lactide) as Coating Agent on the Opsonization, Phagocytosis, and Pharmacokinetics of Biodegradable Nanoparticles. *Biomacromolecules* **2009**, *10*, 408–416.
66. Muro, S.; Garnacho, C.; Champion, J. A.; Leferovich, J.; Gajewski, C.; Schuchman, E. H.; Mitragotri, S.; Muzykantov, V. R. Control of Endothelial Targeting and Intracellular Delivery of Therapeutic Enzymes by Modulating the Size and Shape of ICAM-1-Targeted Carriers. *Mol. Ther.* **2008**, *16*, 1450–1458.
67. Kozlovskaya, V.; Zavgorodnya, O.; Wang, Y.; Ankner, J. F.; Kharlampieva, E. Tailoring Architecture of Nanothin Hydrogels: Effect of Layering on pH-Triggered Swelling. *ACS Macro Lett.* **2013**, *2*, 226–229.
68. Shuvaev, V. V.; Ilies, M. A.; Simone, E.; Zaitsev, S.; Kim, Y.; Cai, S.; Mahmud, A.; Dziubla, T.; Muro, S.; Discher, D. E.; Muzykantov, V. R. Endothelial Targeting of Antibody-Decorated Polymeric Filomicelles. *ACS Nano* **2011**, *5*, 6991–6999.
69. Serda, R. E.; Mack, A.; Pulikkathara, M.; Zaske, A. M.; Chiappini, C.; Fakhoury, J.; Webb, D.; Godin, B.; Conyers, J. L.; Liu, X.; *et al*. Cellular Association and Assembly of a Multistage Delivery System. *Small* **2010**, *6*, 1329–1340.
70. Yan, Y.; Johnston, A. P. R.; Dodds, S. J.; Kamphuis, M. M. J.; Ferguson, C.; Parton, R. G.; Nice, E. C.; Heath, J. K.; Caruso, F. Uptake and Intracellular Fate of Disulfide-Bonded Polymer Hydrogel Capsules for Doxorubicin Delivery to Colorectal Cancer Cells. *ACS Nano* **2010**, *4*, 2928–2936.
71. Zelikin, A. N.; Breheney, K.; Robert, R.; Tjipto, E.; Wark, K. Cytotoxicity and Internalization of Polymer Hydrogel Capsules by Mammalian Cells. *Biomacromolecules* **2010**, *11*, 2123–2129.
72. Bhowmick, T.; Berk, E.; Cui, X.; Muzykantov, V. R.; Muro, S. Effect of Flow on Endothelial Endocytosis of Nanocarriers Targeted to ICAM-1. *J. Controlled Release* **2012**, *157*, 485–492.
73. Decuzzi, P.; Godin, B.; Tanaka, T.; Lee, S. Y.; Chiappini, C.; Liu, X.; Ferrari, M. Size and Shape Effects in the Biodistribution of Intravascularly Injected Particles. *J. Controlled Release* **2010**, *141*, 320–327.
74. Zhang, Y.; Tekobo, S.; Tu, Y.; Zhou, Q.; Jin, X.; Dergunov, S. A.; Pinkhassik, E.; Yan, B. Permission to Enter Cell by Shape: Nanodisk vs Nanosphere. *ACS Appl. Mater. Interfaces* **2012**, *4*, 4099–4105.
75. Voets, T.; Droogmans, G.; Raskin, G.; Eggermont, J.; Nilius, B. Reduced Intracellular Ionic Strength as the Initial Trigger for Activation of Endothelial Volume-Regulated Anion Channels. *Proc. Natl. Acad. Sci. U.S.A.* **1999**, *96*, 5298–5303.
76. Mouat, M. F.; Manchester, K. L. The Intracellular Ionic Strength of Red Cells and the Influence of Complex Formation. *Comp. Haematol. Int.* **1998**, *8*, 58–60.
77. Demaurex, N. pH Homeostasis of Cellular Organelles. *News Physiol. Sci.* **2002**, *17*, 1–5.
78. Koval, M.; Preiter, K.; Adles, C.; Stahl, P. D.; Steinberg, T. H. Size of IgG-Opsonized Particles Determines Macrophage Response during Internalization. *Exp. Cell. Res.* **1998**, *242*, 265–273.
79. Rejman, J.; Oberle, V.; Zuhorn, I. S.; Hoekstra, D. Size-Dependent Internalization of Particles *via* the Pathways of Clathrin- and Caveolae-Mediated Endocytosis. *Biochem. J.* **2004**, *377*, 159–169.
80. Kastl, L.; Sasse, D.; Wulf, V.; Hartmann, R.; Mircheski, J.; Ranke, C.; Carregal-Romero, S.; Martinez-Lopez, J. A.; Fernandez-Chacon, R.; Parak, W. J.; *et al*. Multiple Internalization Pathways of Polyelectrolyte Multilayer Capsules into Mammalian Cells. *ACS Nano* **2013**, *7*, 6605–6618.
81. Muro, S.; Koval, M.; Muzykantov, V. Endothelial Endocytic Pathways: Gates for Vascular Drug Delivery. *Curr. Vasc. Pharmacol.* **2004**, *2*, 281–299.
82. Han, J.; Zern, B. J.; Shuvaev, V. V.; Davies, P. F.; Muro, S.; Muzykantov, V. R. Acute and Chronic Shear Stress Differently Regulate Endothelial Internalization of Nanocarriers Targeted to Platelet-Endothelial Cell Adhesion Molecule-1. *ACS Nano* **2012**, *6*, 8824–8836.